RSC Advances

PAPER

Cite this: *RSC Adv.*, 2015, **5**, 88928

An approach to prepare nanosized HZSM-22 with enhanced lifetime in the methanol to hydrocarbon (MTH) reaction

Jinbang Wang,[abd] Shutao Xu,[a] Jinzhe Li,[a] Yuchun Zhi,[a] Mozhi Zhang,[ad] Yanli He,[a] Yingxu Wei,*[a] Xinwen Guo[b] and Zhongmin Liu*[ac]

Received 9th September 2015
Accepted 14th October 2015

DOI: 10.1039/c5ra18438j

www.rsc.org/advances

Nanosized HZSM-22 has been successfully prepared using ball milling combined with alkaline and acid leaching treatment. The samples were characterized by XRD, XRF, nitrogen physical adsorption–desorption, SEM and solid state NMR. The results showed that the size of the zeolite crystal was greatly reduced after ball milling treatment, and that the crystallinity of the milled sample can be almost totally restored after further alkaline and acid treatment. The prepared nanosized HZSM-22 exhibited enhanced catalytic stability compared with the parent sample in the MTH reaction. Detailed product analysis implied that the improvement of the diffusion effect and the correspondingly reduced secondary reaction would be the most important factor for the long-term MTH operation over the nanosized catalyst.

1. Introduction

Liquid fuels and olefins are the most important petrochemical products in modern industry and the majority of them are produced from oil resources. The shortage of the resources and the increasing demand for fuels and olefins drive the non-petrochemical route development for the production of these petrochemical commodities. MTH process over acidic zeolites has been developed as the most successfully non-petrochemical route for olefins/gasoline production from the alternative and abundant resources, such as coal, natural gas, biomass or carbon dioxide under proper operation conditions.[1–5] Over the past four decades, there have been numerous publications on MTH reaction over a large variety of zeolites and zeotype molecular sieves with different topologies.[2,6] SAPO-34 (CHA topology) with small 8-membered ring pore openings and large cages has been employed in the commercialized MTO (methanol-to-olefins) process,[7] while ZSM-5 (MFI topology) with 10-membered ring and channel intersections has been used for the industrialized MTP (methanol-to-propene)[8] and MTG (methanol-to-gasoline) process.[9]

ZSM-22, a zeolite with TON topology firstly synthesized by Dwyer, features 1-dimensional 10-membered ring (0.46 × 0.57 nm) channels running parallel to *001* direction.[10] ZSM-22 has been utilized as a catalyst for hydroisomerization dewaxing process, exhibiting high mono-branching selectivity due to pore mouth catalysis.[11] Besides, its application in the conversion of methanol has been also intensively studied recently.[12–19] Cui and coworkers investigated the MTO reaction over ZSM-11 (MEL), ZSM-22 (TON), SAPO-34 (CHA), and SAPO-5 (AFI) and found that ZSM-22 was not reactive for MTO reaction.[12] The authors attributed this phenomenon to the absence of large cross-channel or cage structures which could offer large space to accommodate hydrocarbon pool species.[12–14] In contrast, other studies indicated that methanol conversion over ZSM-22 presented comparable conversion as that of SAPO-34 and that the products were composed of a majority of branched-chain C_5^+ hydrocarbons and very little content of aromatics.[15–18] However, compared to ZSM-5, methanol conversion over ZSM-22 suffers rapid deactivation due to the diffusion limitation of the reactants and products during the reaction, caused by the narrow 1-dimensional and 10-membered ring microporous structure.[20,21] To overcome the mass transfer limitation, the application of molecular sieves with small particle size or hierarchical structure has been one of the potential strategies to prolong the catalyst life span *via* shortening the diffusion paths of the molecular in the catalysts.[22–24] The typical ZSM-22 zeolite prepared by traditional hydrothermal synthesis method exists as needle/rod-shaped submicron particles with the dimension of 1–5 μm in length.[10,16,25–32] Very recently, nanosized ZSM-22

[a]*National Engineering Laboratory for Methanol to Olefins, State Energy Low Carbon Catalysis and Engineering R&D Center, Dalian National Laboratory for Clean Energy, iChEM (Collaborative Innovation Center of Chemistry for Energy Materials), Dalian Institute of Chemical Physics, Chinese Academy of Sciences, Dalian 116023, P. R. China. E-mail: liuzm@dicp.ac.cn; weiyx@dicp.ac.cn; Fax: +86 41184691570; Tel: +86 41184379335*

[b]*State Key Laboratory of Fine Chemicals, PSU-DUT Joint Center for Energy Research, School of Chemical Engineering, Dalian University of Technology, Dalian 116024, P. R. China*

[c]*State Key Laboratory of Catalysis, Dalian Institute of Chemical Physics, Chinese Academy of Sciences, Dalian 116023, P. R. China*

[d]*University of Chinese Academy of Sciences, Beijing 100049, P. R. China*

with length of 100 nm has been firstly synthesized by Oki Muraza and coworkers in hydrothermal system with horizontal rotation.[19] Besides, mesopore has be introduced into ZSM-22 by desilication with alkaline solution to enhance the capacity of the carbonaceous species accommodation at the expense of the 60% original Brønsted acid site,[33] moreover, the desilication efficiency for ZSM-22 was much lower than that of ZSM-5.[34,35]

Recently, bead milling, as a physical method, was proposed to prepare nanosized zeolites, such as ZSM-5, zeolite A, zeolite X, and SAPO-34.[36–40] According to these reports, the large zeolite particles could be destroyed by ball milling into fines with crystalline phase and damaged parts, and then the latter could be washed off by the following alkaline leaching process or be remedied by recrystallization in a dilute silicate solution.[36–40]

In the present work, nanosized ZSM-22 with high crystallinity was successfully prepared using a facile approach, bead milling and following mild basic and acidic treatment. The length of ZSM-22 running parallel to *001* direction was significantly shortened without changing the Si/Al ratio and acidity of the zeolite. The lifetime of MTH reaction over nanosized HZSM-22 was prolonged dramatically as about 8 times as that of the parent HZSM-22, meanwhile the product selectivity was comparable with that before milling treatment.

2. Experiment

2.1. Catalysts preparation

The catalyst of ZSM-22 was calcinated at 600 °C for 10 h to remove the template and marked as ZSM-22(P). 10 g ZSM-22(P) and 25 ml deionized water were mixed and then milled at 500 rpm for 5 h using ball mill instrument of QM-3SP2 planetary. Half of the agate jar was filled with agate balls with diameter of 3, 6 and 10 mm. After milling, the suspension in the jar was gathered and dried at 110 °C overnight. The obtained solid sample was designated as ZSM-22-M.

5 g ZSM-22-M sample was added into a beaker flask containing 100 ml 0.5 M NaOH solution. The mixture was heated with a water bath at 65 °C for 30 min under stirring and then washed three times with deionized water. After being dried overnight, the alkaline treated ZSM-22-M was mixed well with 100 ml 0.2 M HCl solution and treated at 65 °C for 6 h under stirring. After being washed and dried, the final sample with alkaline and acid treatment was marked as ZSM-22-M-A-A.

For comparison, 5 g ZSM-22(P) also underwent the same basic and acid treatment as that of ZSM-22-M-A-A without milling. The obtained sample was marked as ZSM-22-A-A.

All the samples were converted into H-form zeolite by 3 times ion exchange at 80 °C for 6 h in 1 M NH_4NO_3 solution, followed by being washed with deionized water, dried at 120 °C for 12 h and calcined at 550 °C for 4 h.

2.2. Catalysts characterization

The crystallinity of the H-form samples were characterized using a PANalytical X'Pert PRO X-ray diffraction (XRD) meter with Cu-Kα radiation ($\lambda = 1.54059$ Å) at 40 kV and 40 mA. The chemical composition of the catalysts was determined by Philips Magix-601 X-ray fluorescence (XRF) spectrometer. The morphology and particle size of the catalysts were measured by field emission scanning electron microscopy (FE-SEM, Hitachi, SU8020). The sample crystal size was further determined on a Zetasizer nano laser particle size analyzer. Nitrogen adsorption–desorption isotherms were obtained on a Micrometrics ASAP 2020 system at 77 K. The total surface area was calculated based on the Brunauer–Emmett–Teller (BET) equation. The micropore volume and micropore surface area was evaluated with *t*-plot method. The mesopore volume was calculated by BJH method. All the solid state NMR experiments were performed on a Bruker AvanceIII 600 spectrometer equipped with a 14.1 T wide-bore magnet. The resonance frequencies were 600.13, 156.4 and 119.2 MHz for ^{1}H, ^{27}Al and ^{29}Si, respectively. The acidity of the H-ZSM-22 catalyst was determined by temperature programmed desorption of ammonia (NH_3-TPD) on a chemical adsorption instrument (Micromeritics AutoChem 2920). The sample (0.14 g) was loaded in a U-shaped microreactor and pretreated at 650 °C for 30 min under helium atmosphere. After cooling to 100 °C, the sample was saturated with ammonia, followed by purging with helium to remove physisorbed ammonia. The ammonia desorption was carried out in helium flow (40 ml min^{-1}) by increasing the temperature from 100 to 600 °C with a heating rate of 10 °C min^{-1} and monitored by a thermal conductivity detector (TCD).

2.3. Catalytic test

50 mg catalyst was pressed, sieved to 40–60 mesh and loaded in a fixed-bed quartz tubular reactor with inner diameter of 4 mm. Prior to the reaction, the catalyst was activated at 500 °C for 40 min, and then the temperature was adjusted to 400 °C. Methanol was fed by passing the carrier gas (12.4 ml min^{-1}) through a saturator containing methanol at 14 °C, which gave a WHSV of 2.0 g g^{-1} h^{-1}. Methanol conversion was performed under atmospheric pressure. The effluent products from reactor were kept warm and analyzed by online gas chromatography equipped with a PoraPLOT Q-HT capillary column and a FID detector. The conversion and selectivity were calculated on CH_2 basis. Dimethyl ether (DME) was considered as reactant in the calculation.

After the reaction, the discharged catalyst was cooled quickly by putting them into the vessel containing liquid nitrogen, and divided into two parts. One part was used for thermogravimetric analysis (TGA) performed on a thermogravmetric analyzer (Q600 SDT/OmniStar). 10–15 mg of deactivated samples was placed into a Al_2O_3 crucible and then heated from ambient temperature to 900 °C at a rate of 10 °C with a purging air flow of 100 ml min^{-1}. 25 mg deactivated samples of the other part was transferred into a Teflon vial and dissolved in 1 ml 20% HF solution for 30 min. The organic species, extracted by 0.5 ml dichloromethane, were analyzed by GC-MS (Agilent 7890A/5975C MSD) with a HP-5 MS capillary column (30 m × 0.25 mm, 0.25 μm).

For the reaction of methanol conversion, methanol conversion (C (%)) and products selectivities (S (%)) were calculated based on eqn (1) and (2), respectively:

$$C = \frac{(1 - \mathrm{wt_{MeOH}\%} - \mathrm{wt_{DME}\%})/14}{(1 - \mathrm{wt_{MeOH}\%} - \mathrm{wt_{DME}\%})/14 + (\mathrm{wt_{MeOH}\%}/32) + (\mathrm{wt_{DME}\%}/23)} \times 100\% \quad (1)$$

$$S_x = \frac{\mathrm{wt}_x\%/14}{(1 - \mathrm{wt_{MeOH}\%} - \mathrm{wt_{DME}\%})/14} \times 100\%. \quad (2)$$

3. Results and discussion

3.1. Catalysts characterization

Fig. 1 displays the FE-SEM images of (a) HZSM-22(P), (b) HZSM-22-A-A, (c) HZSM-22-M and (d) HZSM-22-M-A-A. Despite that some crystals align or fuse sideways, the HZSM-22(P) particles display typically rod-like morphology.[41] The length of aggregated ZSM-22(P) particles is about 1 μm as shown in Fig. 1(a), which is also confirmed by the particle size distribution in Fig. 2, measured by nano laser particle size analyzer. As presented in SEM image of ZSM-22-A-A in Fig. 1(b), the morphology and particle size of HZSM-22 remain unchanged after alkaline–acid treatment. However, after milling, most of the HZSM-22 particles are well-dispersed and crushed into much shorter and irregular rod-like catalyst particles with length in the range from 50 to 350 nm in Fig. 1(c) and (d). Particle size distribution in Fig. 2 also supported the reduction in crystal size. The average size of HZSM-22-M-A-A is 315 nm, much smaller than that of parent sample (~1000 nm). These results shows that ball milling is a facile and efficient method to prepare nanosized particle catalysts, which is usually difficult to be prepared with conventional one-pot synthesis.[10,16,25–32]

Fig. 3 shows the XRD patterns of HZSM-22(P), HZSM-22-A-A, HZSM-22-M, and HZSM-22-M-A-A. All samples displayed the typical diffraction peaks of TON framework.[10,42] Taking HZSM-22(P) as the reference sample, the relative crystallinity of HZSM-22-A-A, HZSM-22-M and HZSM-22-M-A-A are 102, 59 and 96, respectively, as calculated on basis of the intensity of four typical diffraction peaks in the 2θ range of 20° to 27°. Compared to parent sample HZSM-22(P), the relative crystallinity of HZSM-22-M decreased by 41%, indicating the formation of amorphous phase induced by ball milling. While the crystallinity of the milled catalyst can be recovered from 59% (HZSM-22-M) to 96% (HZSM-22-M-A-A) after successive alkaline and acid treatment. The crystallinity of HZSM-22-A-A (102%) was also slightly improved compared with that of HZSM-22(P) (100%) when HZSM-22(P) underwent the same basic and acidic treatment process without milling. Therefore, alkaline and acid post-treatment herein is proved to be an effective approach to remove amorphous debris from the prepared nano catalyst and then restore the crystallinity of the milled sample.

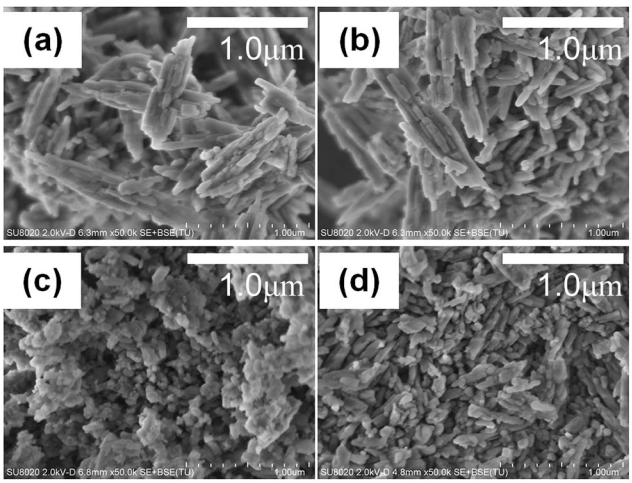

Fig. 1 FE-SEM images of (a) HZSM-22(P), (b) HZSM-22-A-A, (c) HZSM-22-M and (d) HZSM-22-M-A-A.

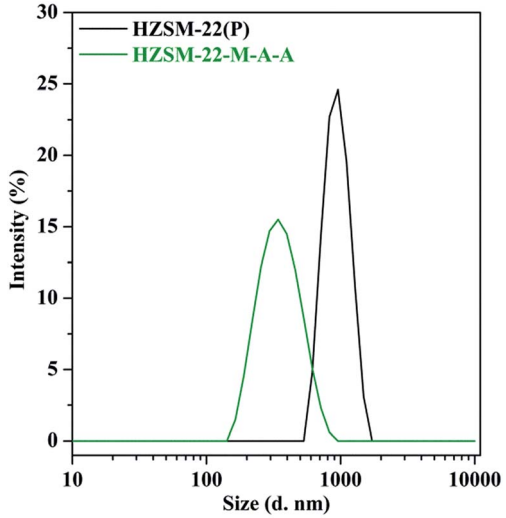

Fig. 2 Particle size distribution of HZSM-22(P) and HZSM-22-M-A-A.

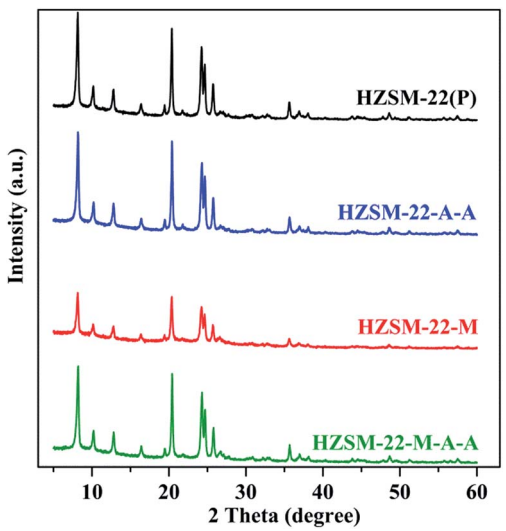

Fig. 3 XRD patterns of HZSM-22(P), HZSM-22-A-A, HZSM-22-M and HZSM-22-M-A-A.

Table 1 Si/Al ratios and acid density of HZSM-22(P), HZSM-22-A-A, HZSM-22-M and HZSM-22-M-A-A

Samples	Si/Al[a]	Si/Al[b]	AlOH[c], mmol g^{-1}	SiOH[c], mmol g^{-1}	Brønsted acid[c], mmol g^{-1}
HZSM-22(P)	34.0	31.8	0.122	0.134	0.327
HZSM-22-A-A	33.8	31.7	0.119	0.129	0.318
HZSM-22-M	35.5	32.1	0.206	0.322	0.199
HZSM-22-M-A-A	36.5	31.4	0.127	0.156	0.304

[a] Determined by XRF. [b] Determined by ^{29}Si MAS NMR. [c] Determined by ^{1}H MAS NMR.

The Si/Al ratios in Table 1, determined by XRF, present very close value among the four samples, indicating that the milling condition and alkaline and acid treatment has little effect on the composition of the HZSM-22 catalysts.

For better understanding of the variation of acidity and element coordination environment of the prepared HZSM-22 catalysts, ^{1}H, ^{27}Al and ^{29}Si MAS NMR spectra of the calcined HZSM-22(P), HZSM-22-A-A, HZSM-22-M and HZSM-22-M-A-A were recorded and shown in Fig. 4. The signals with chemical shifts at −112, −109, −106, −102 and −96 ppm in the ^{29}Si MAS NMR spectra (Fig. 4(c)) are ascribed to two kinds of Si(0Al) (−112 and −109 ppm), Si(1Al), Si(OH) and $Si(OH)_2$ species, respectively.[43] The signals with chemical shifts at 55 and 0 ppm in the ^{27}Al MAS NMR spectrum (Fig. 4(b)) are assigned to framework Al species in tetrahedral coordination state and extra-framework Al species in octahedral coordination state, respectively.[44] Four peaks with chemical shifts at 1.7, 2.5, 3.9 and 6.0 ppm in the ^{1}H MAS NMR (Fig. 4(a)) are attributed to terminal silanol groups (SiOH) on the external surface or at lattice defects, non-acidic extra-framework aluminum hydroxyl groups (EFAl-OH), acidic bridging hydroxyl groups (Si(OH)Al) and disturbed acidic bridging hydroxyl groups (Si(OH)Al) influenced by additional interaction with framework oxygen.[45,46] The data summarized in Table 1 indicated that ball milling gives rise to the decrease of the Brønsted acid density from 0.327 mmol g^{-1} of HZSM-22(P) to 0.199 mmol g^{-1} of HZSM-22-M, and correspondingly the densities of Al–OH and Si–OH increased from 0.122 mmol g^{-1} and 0.134 mmol g^{-1} to 0.206 mmol g^{-1} and 0.322 mmol g^{-1}, respectively. Concurrently, the peaks of tetrahedral framework Al were slightly broadened due to the changes of local chemical environment induced by ball milling treatment (Fig. 4(b)). In addition, the amount of extra-framework Al in HZSM-22-M also increased slightly compared with HZSM-22(P) (Fig. 4(b)). Taken together, these results show that the ball milling treatment can mediate the chemical environment of Al and Si and then alter the acidity. However, these changes could be eliminated by the subsequent alkaline–acid treatment. As shown in Table 1 and Fig. 4, the Brønsted acid densities as well as the Al–OH and Si–OH densities can be recovered back to the level close to the parent sample after the alkaline and acid post-treatment. It should be noted that the alkaline and acid post-treatment without ball milling has little effect on the Al and Si chemical environment of the parent sample as shown in Table 1 and Fig. 4. As for the framework Si/

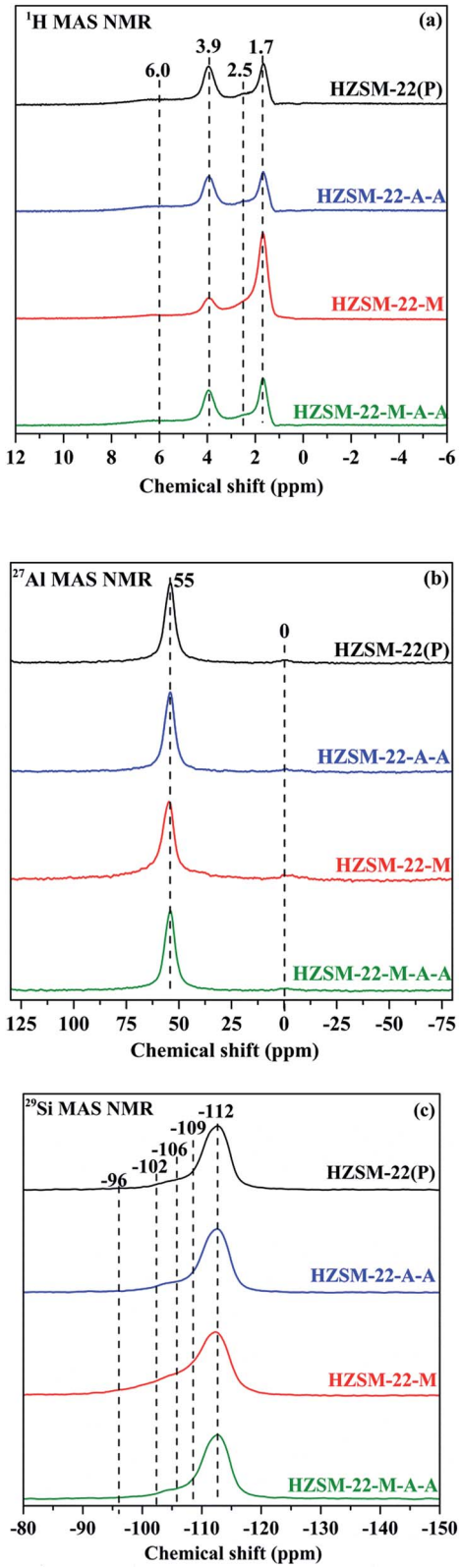

Fig. 4 ^{1}H (a), ^{27}Al (b) and ^{29}Si (c) MAS NMR spectra of the calcined HZSM-22(P), HZSM-22-A-A, HZSM-22-M and HZSM-22-M-A-A.

Al ratio determined by ^{29}Si MAS NMR shown in Table 1, the values of the four samples are close to each other in the range of 31–32, indicating that the alkaline and acid treatment condition applied for removing the amorphous phase has little effect on the crystalline phase. These results further confirmed that ball milling treatment could cause the fragmentation of the zeolite, leading to the reduction of crystallinity and Brønsted acid density, while the loss of crystallinity and Brønsted acidity could be restored by the following base and acid treatment to remove the amorphous fractions.

To further confirm the alteration of acidity of the zeolite resulting from the ball milling and/or the following alkaline and acid treatment, NH_3 adsorption measurement was subsequently performed. The characteristic NH_3 desorption peak centered at 430 °C shown in Fig. 5 represent that the ball milling will lower the acidity of sample, however, the following alkaline and acid treatment can restore the acidity to the level of parent sample. Besides, the acidity of the sample solely subject to the alkaline and acid post-treatment without ball milling is not apparently altered. All these results conform to the acidity change illustrating by the NMR results shown in Fig. 4.

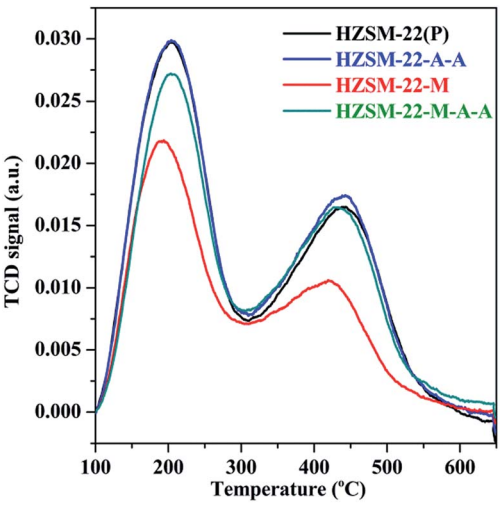

Fig. 5 NH_3-TPD profiles of HZSM-22(P), HZSM-22-A-A, HZSM-22-M and HZSM-22-M-A-A.

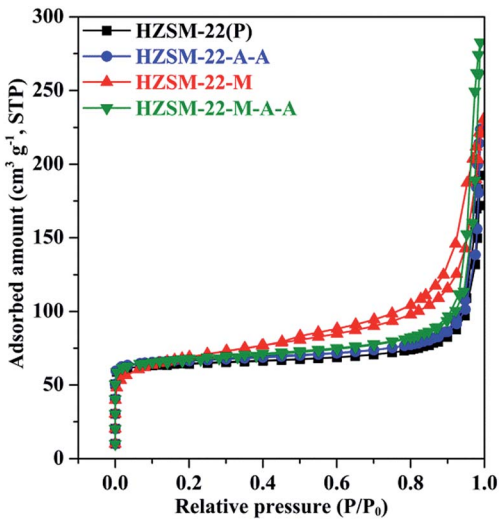

Fig. 6 Nitrogen adsorption and desorption isotherms of HZSM-22(P), HZSM-22-A-A, HZSM-22-M and HZSM-22-M-A-A.

Table 2 Textual properties of HZSM-22(P), HZSM-22-A-A, HZSM-22-M and HZSM-22-M-A-A

Samples	S_{total}[a], $m^2\ g^{-1}$	S_{micro}[b], $m^2\ g^{-1}$	S_{ext}[b], $m^2\ g^{-1}$	V_{micro}[b], $cm^3\ g^{-1}$	V_{meso}[c], $cm^3\ g^{-1}$
HZSM-22(P)	217	185	32	0.086	0.212
HZSM-22-A-A	215	189	36	0.088	0.258
HZSM-22-M	238	119	119	0.054	0.297
HZSM-22-M-A-A	229	176	53	0.082	0.355

[a] BET method. [b] *t*-plot method. [c] BJH method.

Nitrogen adsorption and desorption isotherms of all the samples are shown in Fig. 6 and the textural properties are summarized in Table 2. The parent HZSM-22(P) exhibits typical microporous properties of ZSM-22 with BET surface area of 217 $m^2\ g^{-1}$ (microporous surface area 185 $m^2\ g^{-1}$ and external surface area 32 $m^2\ g^{-1}$) and the weak hysteresis loop is attributed to inter crystal mesopore. Ball milling greatly reduced the microporous surface. HZSM-22-M has a lowered microporous surface area of 119 $m^2\ g^{-1}$ and its external surface area increases to 119 $m^2\ g^{-1}$, and concomitantly the micropore volume of HZSM-22-M decreases from 0.086 $cm^3\ g^{-1}$ of HZSM-22(P) to 0.054 $cm^3\ g^{-1}$. This suggests that part of the zeolite framework has been destroyed into amorphous fragments, causing the blockage of the mircopore channel of zeolites. It should be noted that, after mild basic and acid treatment, the micropore surface area could be restored from 119 $m^2\ g^{-1}$ of HZSM-22-M to 176 $m^2\ g^{-1}$, close to that of the parent sample (~185 $m^2\ g^{-1}$). The same holds true for the micropore volume that was restored from 0.054 $cm^3\ g^{-1}$ of HZSM-22-M to 0.082 $cm^3\ g^{-1}$, comparable with the parent sample (~0.086 $cm^3\ g^{-1}$). The recovery of the microporous surface area and volume implicates that the fabricated fragments of the amorphous debris during ball milling process have been effectively cleared up from the zeolite pores, which concurs with the observation with respect to the restoration of the crystallinity of HZSM-22-M sample after successive alkaline and acid treatment shown in Fig. 3. The hysteresis loops of HZSM-22-M and HZSM-22-M-A-A are more obvious than that of HZSM-22(P) in Fig. 6, reflecting the enlarged mesopore volume from 0.212 $cm^3\ g^{-1}$ of parent sample to 0.258–0.355 $cm^3\ g^{-1}$ detailed in Table 2. This is probably a consequence of inter crystal mesopore formed with the aggregation of the crushed nano particles during ball milling.

3.2. Catalytic performance

The catalytic tests of methanol conversion over the four HZSM-22 catalysts were carried out in a continuous-flow reaction systems and methanol conversions with time-on-stream are shown in Fig. 7. The conversion of MTH reaction over HZSM-

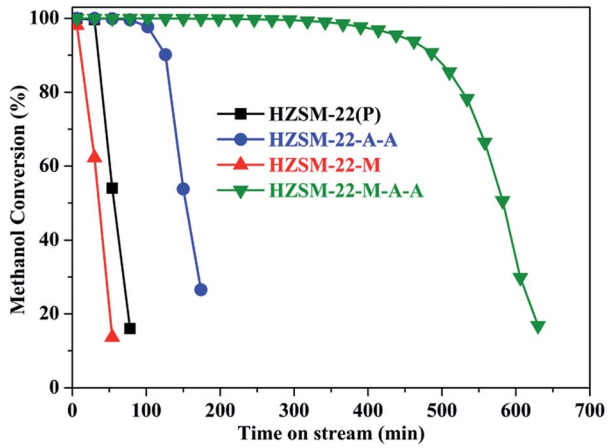

Fig. 7 Methanol conversion variation with time on stream (TOS) over HZSM-22(P), HZSM-22-A-A, HZSM-22-M, and HZSM-22-M-A-A at 400 °C, WHSV = 2 g g^{-1} h^{-1}, and He/methanol = 10.1.

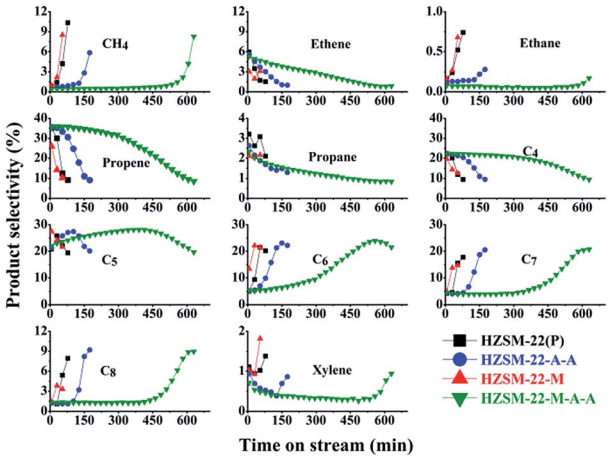

Fig. 8 Product selectivities variation with time on stream (TOS) over HZSM-22(P), HZSM-22-A-A, HZSM-22-M and HZSM-22-M-A-A at 400 °C, WHSV = 2 g g^{-1} h^{-1}, and He/methanol = 10.1.

22(P) decreases from the beginning of the reaction, indicating the quick deactivation of the catalyst. The fast deactivation of the parent zeolite under the relatively low temperature of 400 °C is attributed to the quick formation of heavier aromatics that covers the acid sites and also blocks the pore mouth.[21] More rapid deactivation also occurs over HZSM-22-M. The sharply reduced methanol conversion of HZSM-22-M can be correlated to the partial amorphization of HZSM-22 catalyst during ball milling, which causes the micropore blockage and Brønsted acid density reduction as indicated in the of XRD pattern (Fig. 3), ^{1}H MAS NMR spectra (Fig. 4(a)) and nitrogen adsorption–desorption (Fig. 6). After the following alkaline and acid treatment, the lifetime of HZSM-22-M-A-A was remarkably improved with only 10% reduction in methanol conversion after reaction for 500 min, presenting more excellent catalyst stability than previous reports.[15,18,19] The long catalyst lifetime should be attributed to the enhancement of reactant/product diffusion in the nanosized HZSM-22, which can improve the mass transfer of methanol and avoid the secondary reactions of produced olefin products, such as oligomerization, cyclization and H-transfer, in this way, coke formation can be largely depressed.

For comparison, the parent HZSM-22(P) was also treated with the same alkaline and acid leaching process, but without ball milling. Even some improvement in catalyst stability can be observed (methanol conversion over HZSM-22-A-A decreased to 90% in 150 min), the catalyst lifetime was still much shorter than that of nanosized HZSM-22-M-A-A.

Methanol conversion presented the differences in catalyst life span by the usage of HZSM-22 with varied crystal particle size, while the product distribution at initial 100% conversion was comparable for HZSM-22(P), HZSM-22-A-A, HZSM-22-M and HZSM-22-M-A-A (as shown in Fig. 8). Propene, C_4 and C_5 hydrocarbons appear as the main products. Ethene and other C_5^+ products are also generated with low selectivity. Compared to HZSM-22(P), the selectivities of C_1–C_3 light alkanes and xylene products over HZSM-22-M-A-A are very low, indicating the H-transfer reactions are largely depressed over this treated catalyst with reduced particle size. The evolution of the selectivity profiles with time on stream was similar among the four catalysts. C_2–C_4 alkenes selectivity decreased while C_5^+ selectivity increased to a maximum value and then declined, indicating that the methanol conversion over the four catalysts follows the same reaction and deactivation mechanism. In this study, it is more reasonable to attribute the enhancement of catalyst lifetime of HZSM-22-M-A-A to the diffusion effect improved by reducing the crystal size.

3.3. Analysis of retained coke species in deactivated catalysts

The deposited coke amounts were determined by TGA experiments and the detailed coke species retained within the four deactivated catalysts after the MTH reaction were identified

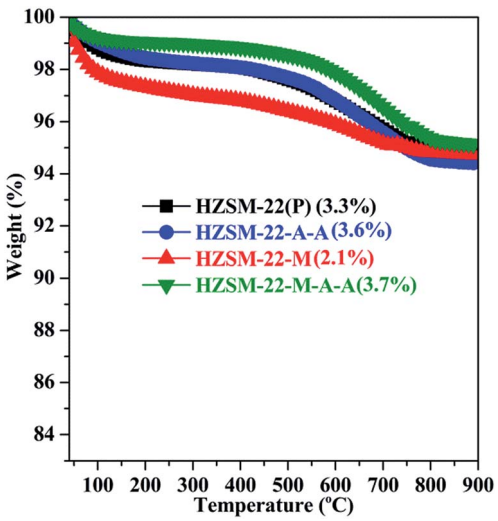

Fig. 9 TGA curves of deactivated HZSM-22(P), HZSM-22-A-A, HZSM-22-M and HZSM-22-M-A-A obtained after MTH reaction at 400 °C, WHSV = 2 g g^{-1} h^{-1}, and He/methanol = 10.1.

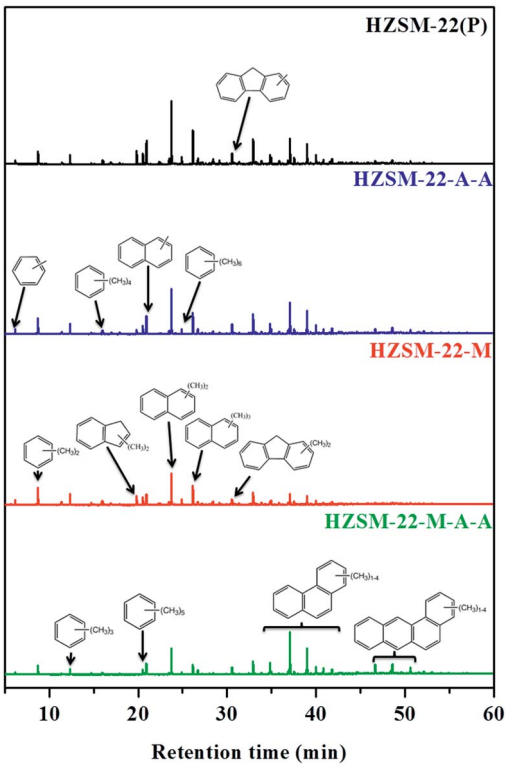

Fig. 10 GC-MS total ion chromatograms of organic species extracts within deactivated HZSM-22(P), HZSM-22-A-A, HZSM-22-M and HZSM-22-M-A-A obtained after MTH reaction at 400 °C, WHSV = 2 g g^{-1} h^{-1}, and He/methanol = 10.1.

with GC-MS analysis. As shown in Fig. 9, the TGA results showed that the amount of deposited coke in HZSM-22(P), HZSM-22-A-A, and HZSM-22-M-A-A was 3.3%, 3.6% and 3.7 wt%, respectively, which was close to each other. The lowest amount of coke within ZSM-22-M (2.1%) was ascribed to the dramatic decrease in the capacity of coke accommodation, resulting from the partial blockage of micropore by amorphous species after ball milling treatment (Table 2). Considering the difference of catalytic lifetime of the four catalysts, nano HZSM-22-M-A-A prepared by ball milling and post alkaline–acid treatment has the lowest methanol consumption on coke formation. According to the GC-MS chromatograms depicted in Fig. 10, the deposited coke species are mostly composed of benzene, naphthalene, phenanthrene, tetraphene and their methyl-substituted derivatives. It is worthy to note that more methyl-substituted phenanthrene and tetraphene were formed over deactivated HZSM-22-M-A-A than other three catalysts. It is supposed that these bulky aromatics are accommodated near the pore mouth of 10-membered ring channel of HZSM-22 due to their bulky nature. Nano crystals preparation with ball milling makes more 1-dimensional and 10-membered ring channel open to the external surface. Besides accommodating larger fused aromatics in the MTH reactions, the usage of nano crystals as MTH catalyst improves the accessibility of the reactant and also accelerates the exiting of the generated products. In this way, the lifetime of MTH reaction over HZSM-22-M-A-A can be greatly prolonged.

4. Conclusions

In summary, nanosized ZSM-22 has been prepared successfully by the combination of ball milling and alkaline and acid post treatment. This method is more advantageous than other strategies because it could effectively shorten the crystal length of HZSM-22 into nanoscale in *001* direction without changing the framework Si/Al ratio and crystallinity. More importantly, the prepared nanosized HZSM-22 exhibited significantly enhanced lifetime in the MTH reactions with similar product selectivity compared with the parent HZSM-22. The shortened diffusion pathway of reactant and products within 1-dimensional and 10-membered ring channel and the resulting depression of H-transfer reactions contribute to the long-term lifetime of nanosized catalyst, HZSM-22-M-A-A.

Acknowledgements

We thank the financial support from National Natural Science Foundation of China (21473182, 21273005, 21273230 and 21103180).

Notes and references

1 H. M. Torres Galvis and K. P. de Jong, *ACS Catal.*, 2013, **3**, 2130–2149.
2 U. Olsbye, S. Svelle, M. Bjørgen, P. Beato, T. V. W. Janssens, F. Joensen, S. Bordiga and K. P. Lillerud, *Angew. Chem., Int. Ed.*, 2012, **51**, 5810–5831.
3 M. Stöcker, *Microporous Mesoporous Mater.*, 1999, **29**, 3–48.
4 T. Xu, H. Song, W. P. Deng, Q. H. Zhang and Y. Wang, *Chin. J. Catal.*, 2013, **34**, 2047–2056.
5 L. Wu, Z. Y. Liu, L. Xia, M. H. Qiu, X. Liu, H. J. Zhu and Y. H. Sun, *Chin. J. Catal.*, 2013, **34**, 1348–1356.
6 K. Hemelsoet, J. van der Mynsbrugge, K. de Wispelaere, M. Waroquier and V. van Speybroeck, *ChemPhysChem*, 2013, **14**, 1526–1545.
7 J. Liang, H. Li, S. Zhao, W. Guo, R. Wang and M. Ying, *Appl. Catal.*, 1990, **64**, 31–40.
8 H. Koempel and W. Liebner, *Stud. Surf. Sci. Catal.*, 2007, **167**, 261–267.
9 C. D. Chang and A. J. Silvestri, *J. Catal.*, 1977, **47**, 249–259.
10 G. T. Kokotailo, J. L. Schlenker, F. G. Dwyer and E. W. Valyocsik, *Zeolites*, 1985, **5**, 349–351.
11 J. A. Martens, W. Souverijns, W. Verrelst, R. Parton, G. F. Froment and P. A. Jacobs, *Angew. Chem., Int. Ed. Engl.*, 1995, **34**, 2528–2530.
12 Z. M. Cui, Q. Liu, W. G. Song and L. J. Wan, *Angew. Chem., Int. Ed.*, 2006, **45**, 6512–6515.
13 Z. Cui, Q. Liu, Z. Ma, S. Bian and W. Song, *J. Catal.*, 2008, **258**, 83–86.
14 Q. Wang, Z.-M. Cui, C.-Y. Cao and W.-G. Song, *J. Phys. Chem. C*, 2011, **115**, 24987–24992.
15 S. Teketel, S. Svelle, K.-P. Lillerud and U. Olsbye, *ChemCatChem*, 2009, **1**, 78–81.

16 S. Teketel, W. Skistad, S. Benard, U. Olsbye, K. P. Lillerud, P. Beato and S. Svelle, *ACS Catal.*, 2012, **2**, 26–37.
17 J. Li, Y. Wei, G. Liu, Y. Qi, P. Tian, B. Li, Y. He and Z. Liu, *Catal. Today*, 2011, **171**, 221–228.
18 J. Li, Y. Wei, Y. Qi, P. Tian, B. Li, Y. He, F. Chang, X. Sun and Z. Liu, *Catal. Today*, 2011, **164**, 288–292.
19 A. K. Jamil, O. Muraza, M. Yoshioka, A. M. Al-Amer, Z. H. Yamani and T. Yokoi, *Ind. Eng. Chem. Res.*, 2014, **53**, 19498–19505.
20 D. Verboekend, K. Thomas, M. Milina, S. Mitchell, J. Pérez-Ramírez and J.-P. Gilson, *Catal. Sci. Technol.*, 2011, **1**, 1331.
21 J. Wang, J. Li, S. Xu, Y. Zhi, Y. Wei, Y. He, J. Chen, M. Zhang, Q. Wang, W. Zhang, X. Wu, X. Guo and Z. Liu, *Chin. J. Catal.*, 2015, **36**, 1392–1402.
22 L. Tosheva and V. P. Valtchev, *Chem. Mater.*, 2005, **17**, 2494–2513.
23 K. Na, M. Choi and R. Ryoo, *Microporous Mesoporous Mater.*, 2013, **166**, 3–19.
24 V. Valtchev and L. Tosheva, *Chem. Rev.*, 2013, **113**, 6734–6760.
25 D. Masih, T. Kobayashi and T. Baba, *Chem. Commun.*, 2007, 3303–3305, DOI: 10.1039/b704787h.
26 S. Ernst, J. Weitkamp, J. A. Martens and P. A. Jacobs, *Appl. Catal.*, 1989, **48**, 137–148.
27 R. Kumar and P. Ratnasamy, *J. Catal.*, 1989, **116**, 440–448.
28 N. Kumar, L. E. Lindfors and R. Byggningsbacka, *Appl. Catal., A*, 1996, **139**, 189–199.
29 L.-T. Kong, B.-X. Shen, J.-G. Zhao and J.-C. Liu, *Ind. Eng. Chem. Res.*, 2014, **53**, 16324–16331.
30 M. Chatterjee, D. Bhattacharya, N. Venkatathri and S. Sivasanker, *Catal. Lett.*, 1995, **35**, 313–326.
31 M. W. Simon, S. L. Suib and C. L. Oyoung, *J. Catal.*, 1994, **147**, 484–493.
32 O. Muraza, A. Abdul-lateef, T. Tago, A. B. D. Nandiyanto, H. Konno, Y. Nakasaka, Z. H. Yamani and T. Masuda, *Microporous Mesoporous Mater.*, 2015, **206**, 136–143.
33 D. Verboekend, A. M. Chabaneix, K. Thomas, J.-P. Gilson and J. Pérez-Ramírez, *CrystEngComm*, 2011, **13**, 3408–3416.
34 D. Verboekend and J. Pérez-Ramírez, *Catal. Sci. Technol.*, 2011, **1**, 879–890.
35 D. Verboekend, A. M. Chabaneix, K. Thomas, J.-P. Gilson and J. Pérez-Ramírez, *CrystEngComm*, 2011, **13**, 3408.
36 T. Wakihara, K. Sato, S. Inagaki, J. Tatami, K. Komeya, T. Meguro and Y. Kubota, *ACS Appl. Mater. Interfaces*, 2010, **2**, 2715–2718.
37 T. Wakihara, R. Ichikawa, J. Tatami, A. Endo, K. Yoshida, Y. Sasaki, K. Komeya and T. Meguro, *Cryst. Growth Des.*, 2011, **11**, 955–958.
38 T. Wakihara, A. Ihara, S. Inagaki, J. Tatami, K. Sato, K. Komeya, T. Meguro, Y. Kubota and A. Nakahira, *Cryst. Growth Des.*, 2011, **11**, 5153–5158.
39 T. Wakihara, K. Sato, K. Sato, J. Tatami, S. Kohara, K. Komeya and T. Meguro, *J. Ceram. Soc. Jpn.*, 2012, **120**, 341–343.
40 M. Yang, P. Tian, C. Wang, Y. Yuan, Y. Yang, S. Xu, Y. He and Z. Liu, *Chem. Commun.*, 2014, **50**, 1845–1847.
41 K. Hayasaka, D. Liang, W. Huybrechts, B. R. de Waele, K. J. Houthoofd, P. Eloy, E. M. Gaigneaux, G. van Tendeloo, J. W. Thybaut, G. B. Marin, J. F. Denayer, G. V. Baron, P. A. Jacobs, C. E. Kirschhock and J. A. Martens, *Chemistry*, 2007, **13**, 10070–10077.
42 S. Teketel, W. Skistad, S. Benard, U. Olsbye, K. P. Lillerud, P. Beato and S. Svelle, *ACS Catal.*, 2011, **2**, 26–37.
43 R. Radeglia and G. Engelhardt, *Chem. Phys. Lett.*, 1985, **114**, 28–30.
44 P. Sazama, B. Wichterlova, J. Dedecek, Z. Tvaruzkova, Z. Musilova, L. Palumbo, S. Sklenak and O. Gonsiorova, *Microporous Mesoporous Mater.*, 2011, **143**, 87–96.
45 Y. Jiang, J. Huang, W. Dai and M. Hunger, *Solid State Nucl. Magn. Reson.*, 2011, **39**, 116–141.
46 M. Müller, G. Harvey and R. Prins, *Microporous Mesoporous Mater.*, 2000, **34**, 281–290.